PROCEEDINGS OF SCIENCE

Production and decay of a heavy boson in association with top quarks

Małgorzata Worek[a,*]

[a] *Institute for Theoretical Particle Physics and Cosmology*
RWTH Aachen University, D-52056 Aachen, Germany

E-mail: worek@physik.rwth-aachen.de

We briefly report on NLO QCD corrections to the $pp \to t\bar{t}B+X$ process, where B stands for H, $W^{\pm}$ or Z. In the calculation all double-, single and non-resonant Feynman diagrams, interferences and finite-width effects are included for the top quark and $W^{\pm}/Z$ gauge bosons. Numerical results are shown at the differential cross section level for various factorisation and renormalisation scale settings and a few PDF sets. The main theoretical uncertainties associated with neglected higher-order terms in the perturbative expansion and with different parametrisations of the PDFs are also discussed. Furthermore, we compare our complete predictions for $pp \to t\bar{t}B + X$ in multi-lepton final states to the calculation in the narrow-width approximation.

Loops and Legs in Quantum Field Theory - LL2022,
25-30 April, 2022
Ettal, Germany

*Speaker
†TTK-22-27, P3H-22-076

PoS(LL2022)001

1. Introduction

The associated production of a pair of top quarks with massive gauge bosons in multi-lepton final states has been extensively scrutinised in recent years. From the experimental point of view, an accurate study of $pp \to t\bar{t}W$ and $pp \to t\bar{t}Z$ has become feasible thanks to the increasing amount of data collected at the LHC with $\sqrt{s} = 13$ TeV by ATLAS and CMS [1–5]. From the theoretical perspective, precise predictions for $pp \to t\bar{t}W$ and $pp \to t\bar{t}Z$ are of particular interest because both processes can receive sizeable contributions from physics beyond the Standard Model (SM). In addition, $pp \to t\bar{t}Z$ is the most sensitive process to directly measure the coupling of the top quark to the Z gauge boson. It gives an important insight into top quark properties that is complementary to $t\bar{t}$ and single top quark production as well as to the $t \to Wb$ decay. Any deviations of the coupling strength of the top quark to the Z boson from its SM value might imply the existence of new physics effects. Furthermore, both $pp \to t\bar{t}Z$ and $pp \to t\bar{t}W$ are dominant backgrounds to several searches for new physics as they comprise final states with multiple charged leptons, missing transverse momentum (p_T^{miss}) and b-jets, which are vigorously searched for at the LHC. Last but not least, both processes play a prominent role in the measurements of the SM Higgs boson in $t\bar{t}H$ production with $H \to ZZ \to 4\ell$, $H \to W^+W^- \to 2\ell 2\nu$ and $H \to \tau^+\tau^-$ decays. The $t\bar{t}H$ process, on the other hand, gives a direct window to probe the top quark Yukawa coupling. Even though $pp \to t\bar{t}H$ production contributes only about 1% to the total Higgs boson production cross section, it was observed in 2018 by ATLAS and CMS [6, 7]. In recent measurements of $t\bar{t}H$ and $t\bar{t}W^{\pm}$ production in multi-lepton final states [8, 9], the resulting $t\bar{t}W^{\pm}$ normalisation has been found to be higher than the NLO (QCD + EW) + NNLL theoretical prediction as provided in Ref. [10–13]. Apart from the $t\bar{t}W^{\pm}$ normalisation, a tension in the modelling of the final-state kinematics in the phase-space regions dominated by the $t\bar{t}W^{\pm}$ process has been observed. This tension could not be explained by multipurpose Monte Carlo (MC) generators, which are currently employed by the ATLAS and CMS collaborations. Consequently, the need for more precise theoretical results for $t\bar{t}B$ production is now higher than ever. Such theoretical predictions should include higher order QCD corrections both to the production and decays of top quarks and W gauge bosons as well as $t\bar{t}$ spin correlations at the same level of accuracy.

First next-to-leading order (NLO) QCD calculations for the $pp \to t\bar{t}B + X$ process with $B = H, Z, W^{\pm}$ that meet the above mentioned conditions have been carried out in the narrow-width approximation (NWA) [14–20]. First full NLO QCD computations, which include complete top quark and $W^{\pm}/Z$ off-shell effects for the $pp \to t\bar{t}B+X$ process in the multi-lepton channel, have been provided in Refs. [17, 19–23]. In these computations, off-shell top quarks as well as $W^{\pm}/Z$ gauge bosons have been described by Breit-Wigner propagators. Furthermore, double-, single- as well as non-resonant contributions along with all interference effects have been consistently incorporated at the matrix element level. In a few cases, even NLO electroweak (NLO EW) corrections to the full off-shell $t\bar{t}B + X$ production have been included [24, 25]. A further step towards a more precise modelling of the on-shell $t\bar{t}B + X$ production process has been achieved by including the subleading electroweak corrections [26–28] and improving merging procedures in the presence of one or two additional jets. Finally, a great effort has been made to match $pp \to t\bar{t}B + X$ production to various parton shower programs Refs. [30–37].

In this contribution, we briefly summarise NLO QCD predictions for the $pp \to t\bar{t}B+X$ process

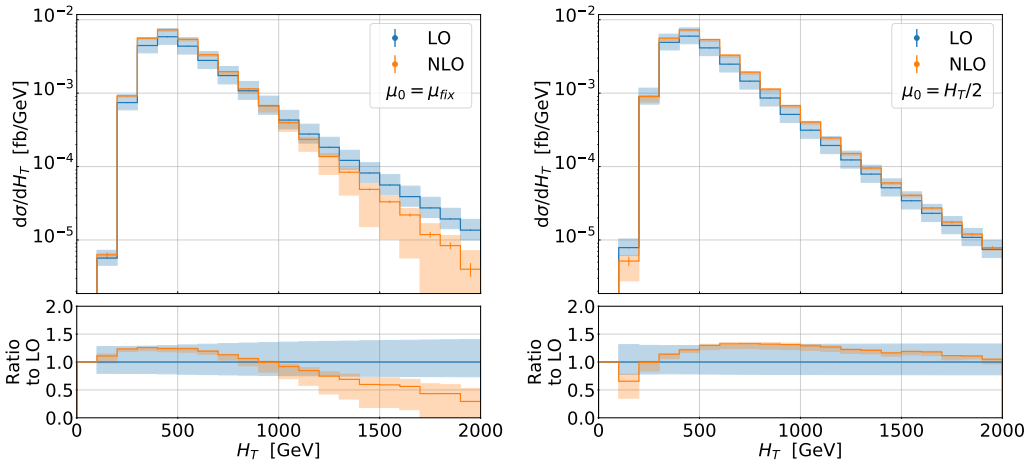

Figure 1: *Differential distributions at LO and NLO in QCD with the corresponding uncertainty bands for the observable H_T for the $pp \to e^+\nu_e\mu^-\bar{\nu}_\mu b\bar{b}H + X$ process at the LHC with $\sqrt{s} = 13$ TeV. Results are presented for $\mu_0 = H_T/2$ and $\mu_0 = \mu_{fix}$. The corresponding scale uncertainty bands as well as Monte Carlo integration errors are also given. The lower panels display the differential $\mathcal{K}$-factor.*

in multi-lepton decay channels. We discuss theoretical results for this process based on full off-shell calculations and the NWA approach. Both types of predictions have been provided with the help of the HELAC-NLO MC package [38] that is built around the HELAC-PHEGAS software [39]. The HELAC-NLO program comprises HELAC-DIPOLES [40, 41], which is used for the calculation of the real emission contributions, as well as HELAC-1LOOP [42], which is employed for the evaluation of the virtual corrections.

2. Differential Cross-Section Results

In the following, we discuss various aspects of higher-order predictions for the $pp \to t\bar{t}B + X$ process at the LHC Run II with $\sqrt{s} = 13$ TeV. We start with assessing the size of the NLO QCD corrections and the perturbative stability of the renormalisation (μ_R) and factorisation (μ_F) scale settings. In Figure 1, we present differential distributions at LO and NLO QCD for the H_T observable defined as $H_T = p_{T,b_1} + p_{T,b_2} + p_{T,e^+} + p_{T,\mu^-} + p_{T,miss} + p_{T,H}$ for the $pp \to e^+\nu_e\mu^-\bar{\nu}_\mu b\bar{b}H + X$ process. Results are presented for $\mu_R = \mu_F = \mu_0$ where $\mu_0 = \mu_{fix} = m_t + m_H/2$ (left panel) and $\mu_0 = H_T/2$ (right panel). Also shown are the corresponding uncertainty bands, which are obtained using a 7-point scale variation, as well as Monte Carlo integration errors. The lower panels display the differential $\mathcal{K}$-factor. The latter is defined according to $\mathcal{K} = \left(d\sigma^{NLO}/dX\right) / \left(d\sigma^{LO}/dX\right)$, where $X = H_T$. All input parameters, PDF sets and restrictions on the kinematics on the final states are given in Ref. [19].

For the fixed scale choice that we employed, $\mu_0 = \mu_{fix} = m_t + m_H/2$, we can observe that for some choices of the ξ parameter, where $\mu_R = \mu_F = \xi\mu_0$, the NLO results become negative. This happens in the high-energy tails of H_T. Furthermore, in the same kinematic regions, scale variation bands at LO and NLO do not overlap anymore. In addition, the scale variation at NLO actually exceeds the scale variation of the LO predictions. At the differential level a fixed

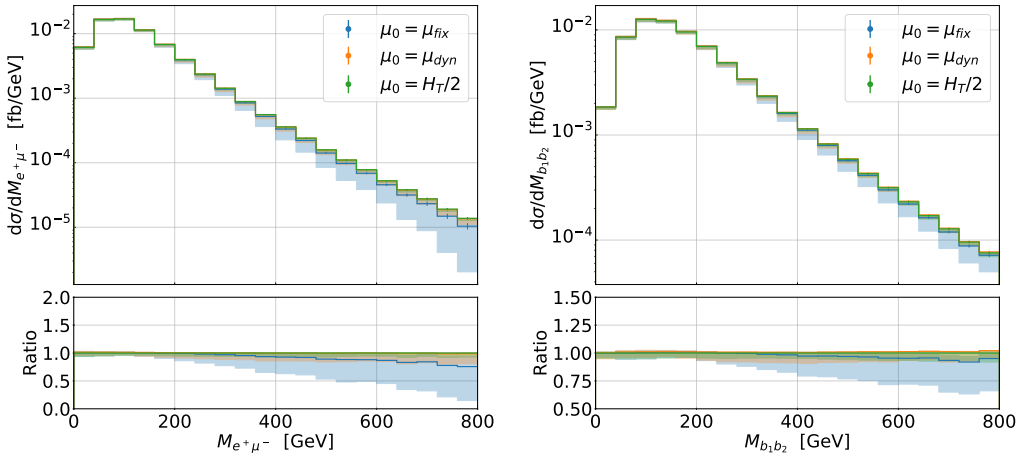

Figure 2: *Differential distributions at NLO QCD for the observables $M_{e^+\mu^-}$ and $M_{b_1b_2}$ for the $pp \to e^+\nu_e\mu^-\bar{\nu}_\mu b\bar{b}H + X$ process at the LHC with $\sqrt{s} = 13$ TeV. Results are shown for three different scale settings: $\mu_0 = \mu_{fix}$, μ_{dyn} and $\mu_0 = H_T/2$. The upper panels show absolute predictions together with the corresponding uncertainty bands resulting from scale variations. Also given are Monte Carlo integration errors. The lower panels display the ratio to the $\mu_0 = H_T/2$ case.*

scale choice cannot handle the dynamics of the process in certain phase-space regions, leading to perturbative instabilities. All these effects, however, might be accommodated by a judicious choice of a dynamical scale setting. For example, for $\mu_0 = H_T/2$, scale uncertainties are well below 10%. In addition, we find that NLO predictions are completely included in the uncertainty bands of the LO prediction. The higher order QCD corrections are not constant in both cases and reach up to 35% even for the dynamical scale setting. Thus, the NLO QCD corrections are necessary for a precise prediction for H_T .

To emphasise the need to use dynamic scale settings even more, we present in Figure 2 NLO differential cross-section distributions for the invariant mass of two leptons ($M_{e^+\mu^-}$) and two b-jets ($M_{b_1b_2}$) for three different scale settings. In addition to $\mu_0 = \mu_{fix}$ and $\mu_0 = H_T/2$ we also plot theoretical predictions for $\mu_0 = \mu_{dyn}$ where $\mu_{dyn} = \left(m_{T,t}\, m_{T,\bar{t}}\, m_{T,H}\right)^{1/3}$ and $m_{T,i} = \sqrt{m_i^2 + p_{T,i}^2}$. We construct top and anti-top momenta directly from their decay products. Scale uncertainties are again displayed as uncertainty bands and the lower panels show the ratio to the results obtained for $\mu_0 = H_T/2$. The two dynamical scales are rather alike for μ_0. The fixed scale setting, however, is quite different already for the central value of the scale. Furthermore, it results in significantly larger scale uncertainties in the tails of dimensionful distributions.

Having examined the size of scale uncertainties for the differential cross-section distributions, we turn our attention to the PDF uncertainties. For this case, we concentrate on the $pp \to e^+\nu_e\mu^-\bar{\nu}_\mu b\bar{b}\tau^+\tau^- + X$ process. All input parameters and the list of selection criteria are summarised in Ref. [20]. In Figure 3 we display the following two observables, the invariant mass of the $\tau^+\tau^-$ system ($M_{\tau^+\tau^-}$) and the transverse momentum of the $\tau^+\tau^-$ system ($p_{T,\tau^+\tau^-}$). We plot them for the CT18 and MMHT14 PDF sets as well as for NNPDF3.1. Each plot comprises three panels. The upper panel displays the absolute NLO prediction for three different PDF sets

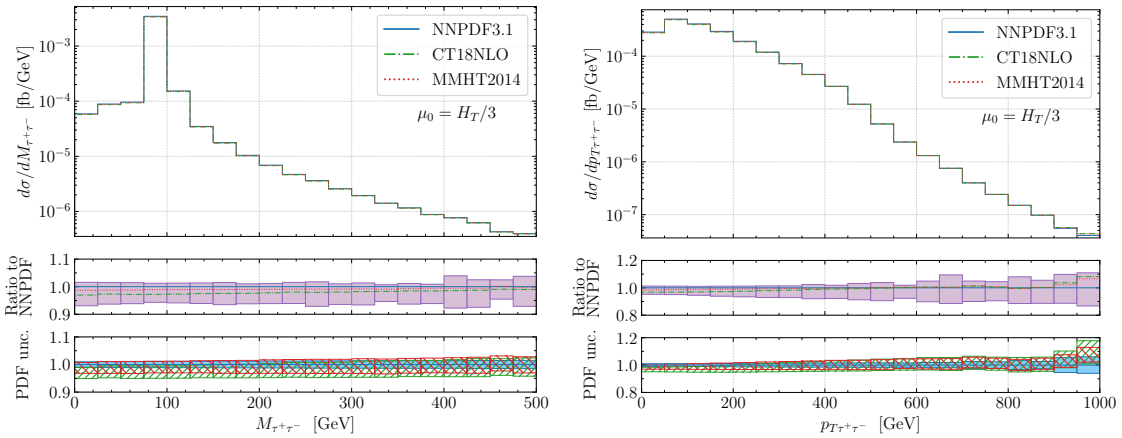

Figure 3: *Differential cross-section distributions for $pp \to e^+\nu_e\mu^-\bar{\nu}_\mu b\bar{b}\tau^+\tau^- + X$ at the LHC with $\sqrt{s} = 13$ TeV as a function of $M_{\tau^+\tau^-}$ and $p_{T\tau^+\tau^-}$. The upper panels show the absolute NLO QCD predictions for three different PDF sets with $\mu_R = \mu_F = \mu_0 = H_T/3$. The middle panels display the ratio to the result with the NNPDF3.1 PDF set as well as its scale dependence. The lower panels present the internal PDF uncertainties for each PDF set.*

at the central scale value, $\mu_R = \mu_F = \mu_0 = H_T/3$ where H_T is defined this time as $H_T = p_{T,b_1} + p_{T,b_2} + p_{T,e^+} + p_{T,\mu^-} + p_{T,\tau^+} + p_{T,\tau^-} + p_T^{miss}$. The middle panel shows the NLO QCD scale dependence band normalised to the NLO prediction obtained with μ_0 and the NNPDF3.1 PDF set. Also given is the ratio of NLO QCD predictions generated for CT18 and MMHT14 to the result calculated with the help of the NNPDF3.1 PDF set. The lower panel displays the internal PDF uncertainties for each PDF set separately, which are also normalised to central NLO predictions with NNPDF3.1. We observe that at the differential level, the NNPDF3.1 PDF uncertainties are very small and well below the corresponding theoretical uncertainties due to scale dependence. When analysing the internal PDF uncertainties for CT18 and MMHT14, we notice that they behave similarly to each other and that their PDF uncertainties are almost a factor of 2 larger than those for NNPDF3.1. Nevertheless, for the selected PDF sets the internal PDF uncertainties are still within the theoretical uncertainties due to scale dependence. Thus, the latter are the dominant source of the theoretical systematics for the differential cross-section distributions at NLO in QCD.

Finally, we examine the size of the non-factorisable corrections for the $pp \to t\bar{t}B + X$ process. To inspect them closely, we compare the NLO QCD results with the complete off-shell effects to the calculations in the NWA. The NWA results are divided into the following two categories: the full NWA and the $\text{NWA}_{\text{LOdecay}}$ case. The full NWA comprises NLO QCD corrections to $t\bar{t}W^\pm$ production and the subsequent top quark decays, preserving at the same time top quark spin correlations. The $\text{NWA}_{\text{LOdecay}}$ case contains the results with NLO QCD corrections to the production stage only, whereas top quark decays are calculated at LO. For consistency, the NWA results with top quark decays at LO are calculated with $\Gamma^{\text{LO}}_{t,\text{NWA}}$.

In general, for very inclusive observables the non-factorisable corrections vanish in the limit

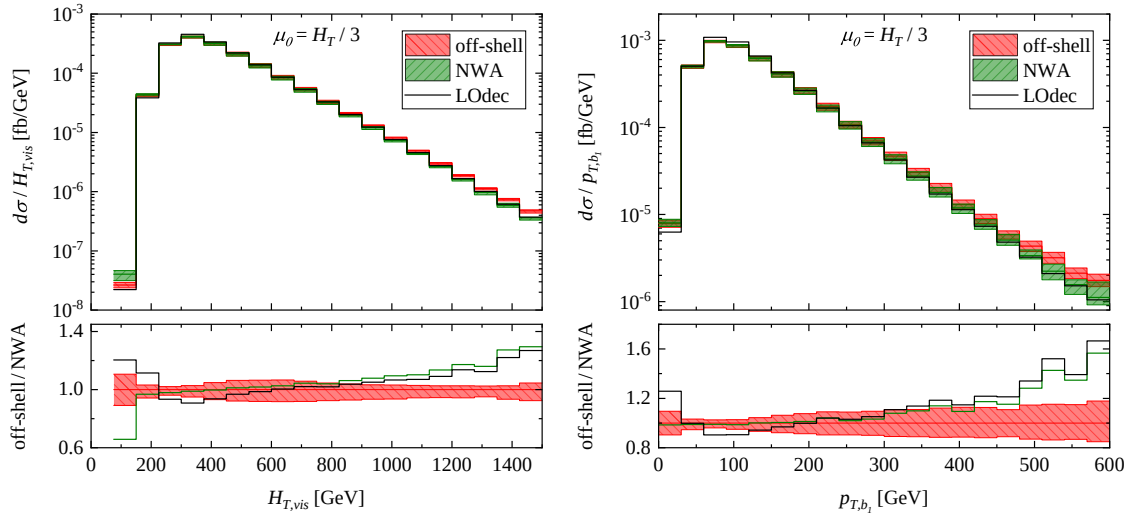

Figure 4: *Differential cross-section distribution as a function of H_T^{vis} and p_{T,b_1} for the $pp \to e^+\nu_e\mu^-\bar{\nu}_\mu e^+\nu_e b\bar{b} + X$ process at the LHC with $\sqrt{s} = 13$ TeV. NLO QCD results for various approaches for the modelling of top quark production and decays are shown. Additionally, theoretical uncertainties as obtained from the scale dependence for the full off-shell case are provided. Also plotted are the ratios of the full off-shell result to the two NWA results.*

$\Gamma/m \to 0$, which satisfies the following hierarchy

$$\frac{\Gamma_Z}{m_Z} > \frac{\Gamma_W}{m_W} > \frac{\Gamma_t}{m_t} \gg \frac{\Gamma_H}{m_H},$$

$$2.7\% > 2.6\% > 0.8\% \gg 0.003\%.$$

Thus, we can expect that the complete off-shell effects are rather small for integrated cross sections for $pp \to t\bar{t}B + X$ production. Indeed, such contributions turn out to be small in inclusive cross sections. However, they are strongly enhanced in some exclusive observables that play an important role in Higgs boson measurements and new physics searches.

In the following, we present our findings for the $pp \to e^+\nu_e\,\mu^-\bar{\nu}_\mu\,e^+\nu_e\,b\bar{b} + X$ process. All input parameters, PDF sets and the cut selection that we have employed can be found in Ref [17]. In Figure 4, we display differential cross-section distribution as a function of H_T^{vis} and p_{T,b_1}. The former observable is defined as $H_T^{vis} = p_T(\mu^-) + p_T(e^+) + p_T(e^+) + p_T(j_{b_1}) + p_T(j_{b_2})$. We plot theoretical results at NLO in QCD for the following three cases, the full NWA, $\text{NWA}_{\text{LOdecay}}$ and full off-shell predictions. For the full off-shell case, we additionally display the theoretical uncertainties as obtained from the scale dependence since we are interested in effects that are outside the NLO uncertainties bands. The upper plots show the absolute predictions at NLO in QCD, whereas the bottom plots display the ratios of the full off-shell result to the two NWA results. We can observe that in the tails of H_T^{vis} and p_{T,b_1}, full off-shell effects increase and are well above the theoretical scale uncertainties. Furthermore, at the beginning of both spectra we can notice large discrepancies between the full NWA description and the $\text{NWA}_{\text{LOdecay}}$ case. They are visible in the phase-space regions that are currently scrutinised by ATLAS and CMS. This highlights the importance of the proper modelling of top quark decays for the $pp \to t\bar{t}B + X$ process.

Overall, in the case of various (dimensionful) differential cross-section distributions for the $pp \to t\bar{t}B + X$ process, non-negligible full off-shell effects are present in various phase-space regions. Substantial differences between the two versions of the NWA results are additionally observed. Taking into account that, a priori, it is not possible to estimate the size of these non-factorisable corrections and which phase-space regions are particularly affected, a very careful examination based on the full theoretical description should be performed on a case-by-case basis. Let us just mention at this point that full off-shell effects also have a significant impact on the top quark mass extraction [43], the charge asymmetry of the top quark and its decay products [44] as well as the calculation of signal strength exclusion limits in $t\bar{t}$ associated Dark Matter production [18].

3. Conclusions

We have briefly summarised NLO QCD corrections to $pp \to t\bar{t}B + X$, where $B = H, Z, W^{\pm}$. In these computations, off-shell top quarks and $W^{\pm}/Z$ have been described by Breit-Wigner distributions. Furthermore, double-, single- as well as non-resonant contributions along with all interference effects have been consistently incorporated at the matrix element level. We have presented our results for the LHC Run II centre of mass system energy of $\sqrt{s} = 13$ TeV for various differential cross-section distributions. We employed several scale settings and three different PDF sets. Large shape distortions have been observed in the presence of higher-order QCD effects. The non-flat differential $\mathcal{K}$-factors underline the importance of NLO QCD corrections for a proper modelling of the $pp \to t\bar{t}B + X$ process kinematics. Furthermore, we have observed that the fixed scale setting led to perturbative instabilities in the TeV regions. The introduction of the dynamical scale stabilises the high p_T tails and generally leads to smaller NLO QCD corrections as well as theoretical uncertainties. In addition, the size of full off-shell effects has been examined. At the differential level, large non-factorisable corrections up to $40\% - 60\%$ have been observed. Last but not least, the differences between the full NWA and $\text{NWA}_{\text{LOdecay}}$ case are substantial, especially in the low p_T regions. The latter phase-space regions are currently scrutinised by ATLAS and CMS. To recapitulate, the non-factorisable NLO QCD corrections as well as higher order QCD effects in top quark decays significantly impact $pp \to t\bar{t}B + X$ cross sections in various phase-space regions. For these reasons, they should be included in future comparisons between theoretical predictions and experimental data.

Acknowledgments

The author would like to thank the organizers of the 16^{th} Workshop on Elementary Particle Physics - *Loops and Legs in Quantum Field Theory* - for a kind invitation and very pleasant atmosphere during the conference.

The work was supported by the Deutsche Forschungsgemeinschaft (DFG) under the following grant: 396021762 - TRR 257: *P3H - Particle Physics Phenomenology after the Higgs Discovery*. Support by a grant of the Bundesministerium für Bildung und Forschung (BMBF) is additionally acknowledged.

References

[1] A. M. Sirunyan *et al.* [CMS], JHEP **08** (2018), 011

[2] M. Aaboud *et al.* [ATLAS], Phys. Rev. D **99** (2019) no.7, 072009

[3] A. M. Sirunyan *et al.* [CMS], JHEP **03** (2020), 056

[4] K. Lee *et al.* [CMS], JHEP **12** (2021), 083

[5] G. Aad *et al.* [ATLAS], Eur. Phys. J. C **81** (2021) no.8, 737

[6] A. M. Sirunyan *et al.* [CMS], Phys. Rev. Lett. **120** (2018) no.23, 231801

[7] M. Aaboud *et al.* [ATLAS], Phys. Lett. B **784** (2018), 173

[8] [ATLAS Collaboration], ATLAS-CONF-2019-045.

[9] [CMS Collaboration], CMS-PAS-TOP-21-011.

[10] A. Broggio, A. Ferroglia, G. Ossola and B. D. Pecjak, JHEP **09** (2016), 089

[11] A. Kulesza *et al.*, Eur. Phys. J. C **79** (2019) no.3, 249

[12] A. Broggio *et al.*, JHEP **08** (2019), 039

[13] A. Kulesza *et al.*, Eur. Phys. J. C **80** (2020) no.5, 428

[14] J. M. Campbell and R. K. Ellis, JHEP **07** (2012), 052

[15] R. Röntsch and M. Schulze, JHEP **07** (2014), 091 [erratum: JHEP **09** (2015), 132]

[16] Y. Zhang, W. G. Ma, R. Y. Zhang, C. Chen and L. Guo, Phys. Lett. B **738** (2014), 1

[17] G. Bevilacqua, H. Y. Bi, H. B. Hartanto, M. Kraus and M. Worek, JHEP **08** (2020), 043

[18] J. Hermann and M. Worek, Eur. Phys. J. C **81** (2021) no.11, 1029

[19] D. Stremmer and M. Worek, JHEP **02** (2022), 196

[20] G. Bevilacqua *et al.*, [arXiv:2203.15688 [hep-ph]].

[21] A. Denner and R. Feger, JHEP **11** (2015), 209

[22] G. Bevilacqua, H. B. Hartanto, M. Kraus, T. Weber and M. Worek, JHEP **11** (2019), 001

[23] A. Denner and G. Pelliccioli, JHEP **11** (2020), 069

[24] A. Denner, J. N. Lang, M. Pellen and S. Uccirati, JHEP **02** (2017), 053

[25] A. Denner and G. Pelliccioli, Eur. Phys. J. C **81** (2021) no.4, 354

[26] J. A. Dror, M. Farina, E. Salvioni and J. Serra, JHEP **01** (2016), 071

[27] R. Frederix, D. Pagani and M. Zaro, JHEP **02** (2018), 031

[28] R. Frederix and I. Tsinikos, Eur. Phys. J. C **80** (2020) no.9, 803

[29] R. Frederix and I. Tsinikos, JHEP **11** (2021), 029

[30] M. V. Garzelli *et al.*, EPL **96** (2011) no.1, 11001

[31] M. V. Garzelli *et al.*, Phys. Rev. D **85** (2012), 074022

[32] M. V. Garzelli, A. Kardos, C. G. Papadopoulos and Z. Trocsanyi, JHEP **11** (2012), 056

[33] H. B. Hartanto, B. Jager, L. Reina and D. Wackeroth, Phys. Rev. D **91** (2015) no.9, 094003

[34] F. Maltoni, D. Pagani and I. Tsinikos, JHEP **02** (2016), 113

[35] F. Febres Cordero, M. Kraus and L. Reina, Phys. Rev. D **103** (2021) no.9, 094014

[36] G. Bevilacqua *et al.*, Phys. Rev. D **105** (2022) no.1, 014018

[37] M. Ghezzi *et al.*, Phys. Rev. D **106** (2022) no.1, 014001

[38] G. Bevilacqua *et al.*, Comput. Phys. Commun. **184** (2013), 986

[39] A. Cafarella, C. G. Papadopoulos and M. Worek, Comput. Phys. Commun. **180** (2009), 1941

[40] M. Czakon, C. G. Papadopoulos and M. Worek, JHEP **08** (2009), 085

[41] G. Bevilacqua, M. Czakon, M. Kubocz and M. Worek, JHEP **10** (2013), 204

[42] A. van Hameren, C. G. Papadopoulos and R. Pittau, JHEP **09** (2009), 106

[43] G. Bevilacqua, H. B. Hartanto, M. Kraus, M. Schulze and M. Worek, JHEP **03** (2018), 169

[44] G. Bevilacqua *et al.*, Eur. Phys. J. C **81** (2021) no.7, 675